11th International Symposium on Magnetic Bearings
August 26-29, Nara, Japan

APPLICATION OF ROTOR UNBALANCE COMPENSATON TO AMB-BASED GYROSCOPIC SENSOR

Yutaka Maruyama, Takeshi Mizuno, Masaya Takasaki
Graduate School of Science & Engineering, Saitama Univ., Saitama, Saitama, 338-8570, Japan
maruyama@mech.saitama-u.ac.jp, mizer@mech.saitama-u.ac.jp, masaya@mech.saitama-u.ac.jp
Yuji Ishino
Innovative Research Organization, Saitama Univ., Saitama, Saitama, 338-8570, Japan
yishino@mech.saitama-u.ac.jp
Hironori Kameno, Atsushi Kubo
Research & Development Center, JTEKT, Kashihara, Nara 634-8555, Japan
hironori_kameno@jtekt.co.jp, atsushi_kubo@jtekt.co.jp

ABSTRACT
An AMB-based gyroscopic sensor is studied in this paper. The sensor has been proposed to realize high-accuracy, compact and low-cost sensors. In this sensor, active magnetic bearing (AMB) is applied to a rate-integrating gyro that measures angular velocity. Two-axis angular velocities are estimated from the control currents canceling gyroscopic torque acting on the AMB rotor. The sensor has detected angular velocity precisely. However, the measured angular velocities include oscillating components due to rotor unbalance. This paper presents an elimination method of the components due to the unbalance.

INTRODUCTON
Gyroscopic sensors (gyros) measure kinematic variables of rigid body based on the inertial effect due to the rotation motion, especially rate gyros measure angular velocity. There are many applications of the gyroscopic sensors in fields of inertial navigation, homing and attitude control. High-accuracy, compact and low-cost gyros are required to achieve sophisticated motion control of robots and unmanned-micro airplanes. The rate gyros are classified into several types according to the detection principle. Vibrating gyros are mostly used for compact and low-cost applications because of the potential in minimization and mass production. Recently, the minimization of the vibrating gyros has been advanced using MEMS technology. However the accuracy of the vibrating gyro is lower than rotating gyros. Although improvements of the accuracy of the vibrating gyros are addressed [1], [2], it is difficult to obtain higher accuracy of the vibrating gyros than the rotating gyros because the detection sensitivity is potentially low due to the small proof mass generating inertial effects. Therefore the vibrating gyros are not suitable for high performance applications. On the other hand, rotating gyros, which utilize the angular momentum of the rotor, maintain a potential to achieve high accuracy because the detection sensitivity increases as increasing spinning rate of the rotor. However the spinning rate is limited due to friction in bearings to support the rotor. Additionally, the rotating gyros have a gimbal mechanism, which supports the rotor with the bearings and guides the rotor about orthogonal axis to the spinning axis. The gimbal mechanism makes the size of the rotating gyros large and requires high precision machining. Such machining increases the production cost. In addition, friction in the other bearings to support the gimbal causes the measurement error [3].
Active magnetic bearing (AMB) has been used in the gimbal to eliminate the friction in the gimbal [4]. AMB-based gyroscopic sensor has been proposed to a realize multi-axis, compact, high-accuracy, and low-cost sensor [5]. AMB itself is utilized as a rotating gyro in this study. There is, therefore, no gimbal mechanism. The rotor is completely non-contact. In addition, two-axis angular velocity and three-axis acceleration generated to the stator are estimated based on the control currents of the AMB. The validation of angular velocity and acceleration measurement has been demonstrated experimentally [6]. However, the measured signals include large noise. This paper shows that major components of the noise are due to rotor unbalance. In addition a method of eliminating the components is presented. In order to eliminate the components, unbalance compensation is applied to the control of the AMB-based gyro. Many unbalance compensation has been proposed such as adaptive force balancing [7], Generalized notch filters [8] and auto balancing [9]. In this study, current regulation control [10] is applied to eliminate the components synchronized with the rotation from the control current and reduces reaction force to the AMB stator. Current

regulation control is suitable for AMB-based gyro due to these features since the angular velocity is estimated based on the control current and the reaction force may obstructs motions of the measurement object. However, the motion of the stator is not consider in the control design although it is assumed to move dynamically. Therefore the efficacy of the current regulation control for the AMB-based gyro is investigated experimentally.

BASIC OF AMB-BASED GYROSCOPIC SENSOR

Active magnetic bearing is applied to the AMB-based gyro. Angular velocities are estimated from the control currents for cancelling the gyroscopic torque. Figure 1 shows a model of AMB-based gyroscopic sensor with rotation of the stator. In this coordinate, the dynamics of an AMB-based gyroscopic sensor are written as follows [6]

$$\begin{cases} \ddot{\theta}_x(t) + a_k\dot{\theta}_y(t) - a_\theta\theta_x(t) \\ \qquad = b_\theta u_{\theta x}(t) - \ddot{\varphi}_x(t) - a_k\dot{\varphi}_y(t), \\ \ddot{\theta}_y(t) - a_k\dot{\theta}_x(t) - a_\theta\theta_y(t) \\ \qquad = b_\theta u_{\theta y}(t) - \ddot{\varphi}_y(t) + a_k\dot{\varphi}_x(t), \end{cases} \tag{1}$$

where $\theta(t)$ is the relative angle of the rotor to the stator, $\varphi(t)$ is the absolute angle of stator, $u_\theta(t)$ is the control current, a_θ is the negative stiffness of electromagnets, b_θ is the conversion coefficient from the current to the angular acceleration. The subscript (x or y) indicates the motion about each axis. a_k is the parameter which presents an effect of gyroscopic action and is given by

$$a_k = I_z\omega_z / I_r, \tag{2}$$

where I_r is the moment of inertia of the rotor about the x- and y-axes, I_z is the moment of inertia about the z-axis, ω_z is the spinning rate of the rotor about the z-axis. Equation (1) demonstrates that motions of the stator act on the dynamics of the relative angle of the rotor to the stator as disturbance. When the rotor is regulated to the stator namely $\theta(t) = 0$, the motions of the stator can be estimated from the control current for canceling the disturbance. The estimation equation is given by

$$\begin{bmatrix} \hat{\Psi}_x(s) \\ \hat{\Psi}_y(s) \end{bmatrix} = \frac{b_\theta}{s^2 + a_k^2}\begin{bmatrix} s & -a_k \\ a_k & s \end{bmatrix}\begin{bmatrix} U_{\theta x}(s) \\ U_{\theta y}(s) \end{bmatrix}, \tag{2}$$

where $\hat{\Psi}(s)$ and $U_\theta(s)$ are the Laplace transforms of the angular velocity $\dot{\varphi}(t)$ and the control current $u_\theta(t)$. However, oscillating components appear in the estimated signal because of the neutral poles ($s = \pm ja_k$) of the transfer function on the right hand side of (2). They may be canceled if a_k in (2) is perfectly identified. The cancellation is, however, imperfect because the spinning rate fluctuates in the actual equipment. Assuming that $\omega << a_k$, (2) can be approximated as

$$\begin{bmatrix} \hat{\Psi}_x(s) \\ \hat{\Psi}_y(s) \end{bmatrix} = \frac{b_\theta}{a_k^2}\begin{bmatrix} s & -a_k \\ a_k & s \end{bmatrix}\begin{bmatrix} U_{\theta x}(s) \\ U_{\theta y}(s) \end{bmatrix}. \tag{3}$$

Therefore, the two-axis angular velocities can be estimated from the control currents about two-axis rotations.

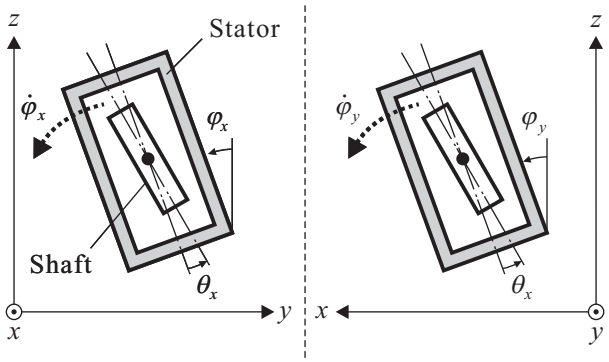

FIGURE 1: Experimental setup for angular velocity measurement.

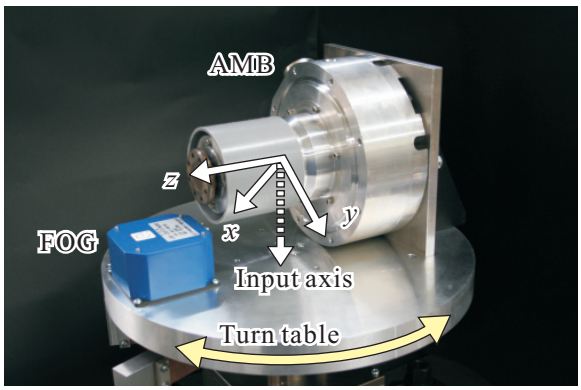

FIGURE 2: Experimental setup for angular velocity measurement.

INFLUENCE OF ROTOR UNBAIANCE

An experimental setup for two-axis angular velocity measurement is shown in Figure 2. Reference signal is generated by a fiber optical gyro (FOG). The performance is specified by dynamic range: ± 10 deg/s, linearity: 1 % FS, bias stability: within 0.03 $(\text{deg/s})_{\text{p-p}}$, bandwidth: 50 Hz. The AMB and the FOG are fixed on the turntable. The center of gravity of the shaft is located above the center of the table. The z-axis points to the horizontal direction. The input axis points to the vertical direction that is at 45 degrees to the x- and y-axes. The same angular velocity is generated about the x- and y-axes. A controller based on the optimal regulator theory is used to control the AMB [11]. An induction motor built in the AMB stator excites the

rotation about z-axis to the rotor. Note that, in induction motors, the rotational speed does not completely synchronize with the frequency of exciting signal in the principle.

Figure 3 shows results of angular velocity measurement using the AMB-based gyroscopic sensor when the stator is swung at the frequency of 1 Hz and amplitude of 1 deg/s simultaneously about both the x- and y-axes. Figure 3 (a) and (b) are the results about the x- and y-axes, respectively. These results demonstrate that the sensor detects the input angular velocities. However, undesirable components are contained in the estimation. The estimations without swinging turntable were carried out so that the cause of the undesirable components was investigated. The spectrums of these estimations are shown in Figure 5. Even without swinging, undesirable components are also included in the estimations about both the x- and y-axes. Therefore the components have nothing with the angular velocities to be measured. In the spectrums, remarkable components common to both x- and y-axes appear. One is a component from a synchronized signal with rotation (159 Hz). Another is due to an exiting signal for spinning the rotor about z-axis (166Hz). The other is a beat (7 Hz) due to these signals. Therefore it is considered that the conical motions due to the rotor unbalance and the excitation cause the undesirable components in the estimated angular velocities. Two higher frequency components (157 and 166 Hz) can be eliminated from the estimated angular velocities by filtering because frequencies of these components are out of the measurement bandwidth of the sensor. On the other hand, the beat component cannot be eliminated from the estimated angular velocities by filtering because the frequency of the beat component is in the measurement bandwidth.

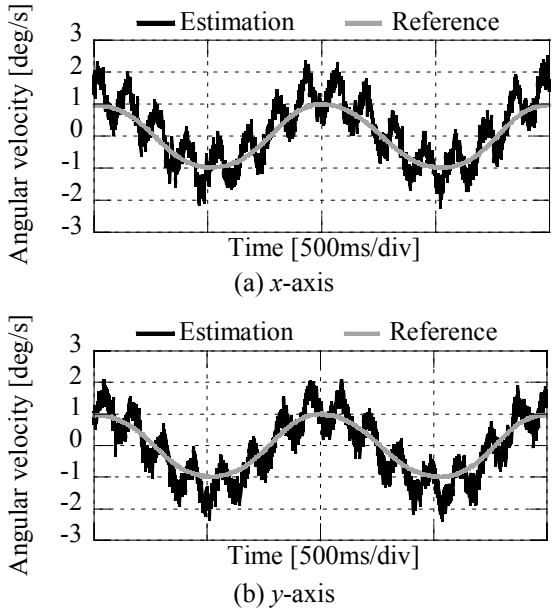

FIGURE 3: Estimated angular velocities with swing at the frequency of 1 Hz, amplitude of 1 deg/s to the stator.

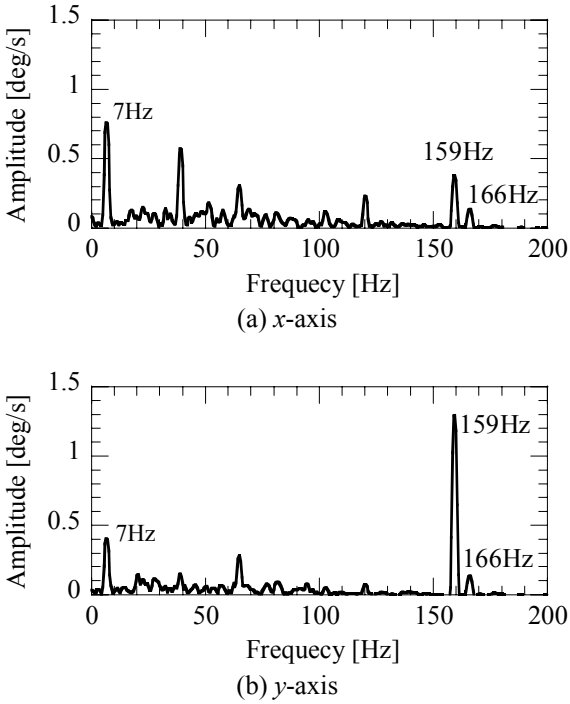

FIGURE 4: Spectrums of estimated angular velocities when the turntable is not swung.

UNBALANCE COMPENSATION

The beat component is eliminated by compensating rotor unbalance, which is a source of the beat. A current regulation control is utilized for rotor unbalance compensation. The current regulation control eliminates a stationary alternating synchronized components with rotation from the control currents. In addition, the rotation about the principal axis of inertia is realized at the high rate spin.

Control Law of Current Regulation Control

When the rotor has mass unbalance, the dynamics of the AMB about the rotations without the motions of the stator are presented as

$$\begin{cases} \ddot{\theta}_x(t) + a_k\dot{\theta}_y(t) - a_\theta\theta_x(t) = b_\theta u_{\theta x}(t) + w_x \,, \\ \ddot{\theta}_y(t) - a_k\dot{\theta}_x(t) - a_\theta\theta_y(t) = b_\theta u_{\theta y}(t) + w_y \,, \end{cases} \tag{4}$$

where $w_x(t)$ and $w_y(t)$ are the unbalance torques. These are given by

$$\begin{cases} w_x = \left(1 - I_z / I_r\right)\tau\omega_z{}^2 \cos(\omega_z t + \beta) \,, \\ w_y = \left(1 - I_z / I_r\right)\tau\omega_z{}^2 \sin(\omega_z t + \beta) \,, \end{cases} \tag{5}$$

where τ is the angle of the rotational axis relative to the

principal axis, β is the initial phase of the projected principal axis on the x-y plane. The unbalance torque is estimated by an observer. These estimations are denoted by $\hat{w}_x$ and $\hat{w}_y$. Although unbalance forces are also generated in the translations, the control about only the rotations is presented in the following because the control in the translation is almost same. Defined complex variables by

$$\begin{cases} u(t) = u_{\theta x}(t) + \boldsymbol{j} u_{\theta y}(t), \\ x(t) = \theta_x(t) + \boldsymbol{j}\theta_y(t), \\ w(t) = w_x(t) + \boldsymbol{j}\, w_y(t), \\ \hat{w}(t) = \hat{w}_x(t) + \boldsymbol{j}\, \hat{w}_y(t). \end{cases} \tag{6}$$

Then Eq. (5) is written as

$$\ddot{x}(t) - \boldsymbol{j} a_k \dot{x}(t) - a_\theta x(t) = b_\theta u(t) + w(t). \tag{7}$$

Denote each Laplace-transformed complex variables by the capital. Then the dynamics of the AMB are written as

$$X(s) = \frac{1}{t_o(s)}\{\, b_\theta U(s) + W(s) \,\}, \tag{8}$$

where $t_o(s)$ is defined as

$$t_o(s) = s^2 - \boldsymbol{j} a_k s - a_\theta. \tag{9}$$

The disturbance due to unbalance is given by

$$W(s) = \frac{w_0}{s - \boldsymbol{j}\omega_z}, \tag{10}$$

where w_0 is the parameter which is determined by the amplitude and initial direction of the unbalance torque. On the other hand, dynamics of the observer for estimating the unbalance torque is given by

$$\hat{W}(s) = \frac{\sigma - \boldsymbol{j}\nu}{s + \sigma - \boldsymbol{j}(\omega_z + \nu)} W(s), \tag{11}$$

where σ and ν are the parameter, which determine the characteristics root of the observer. For convenience, $[A]$ is defined as the coefficient of $(s-\boldsymbol{j}\omega_z)^{-1}$ when $A(s)$ is expanded into partial fraction form. If $A(s)$ has $\boldsymbol{j}\omega_z$ as a simple pole, $[A]$ is given by

$$[A] = \lim_{s \to j\omega_z} (s - \boldsymbol{j}\omega_z)\, A(s). \tag{12}$$

This quantity represents the amplitude and the phase of sinusoidal varying component of $a(t) = \mathcal{L}^{-1}[A(s)]$.
For convenience in analysis, the control current is divided as followings

$$U(t) = U_f(t) + U_w(t), \tag{13}$$

where $U_f(t)$ is the Laplace-transformed feedback current for stabilization, $U_w(t)$ is the Laplace-transformed auxiliary current for unbalance compensation. $U_f(t)$ is determined by the controller as mention in previous section. By using the feedback parameter $K(s)$, $U_f(t)$ is presented as

$$U_f(s) = -K(s)X(s). \tag{14}$$

The feedback parameter $K(s)$ should be decided as stabilizing the following characteristic polynomial.

$$t_c(s) = t_o(s) + b_\theta K(s) \tag{15}$$

Note that the characteristic polynomial has stable poles since the feed parameter is decided based on the optimal regulator theory.
Substituting (13) and (14) into (8), the control current is given by

$$U(s) = -\frac{K(s)}{t_o(s)}\{\, bU(s) + W(s) \,\} + U_w(s). \tag{16}$$

From (16),

$$U(s) = \frac{1}{t_c(s)}\{\, t_o(s)U_w(s) - K(s)W(s) \}. \tag{17}$$

The control current becomes zero completely, when the auxiliary current is decided as follows.

$$U_w(s) = \frac{K(s)}{t_o(s)} W(s) \tag{18}$$

However, $\hat{W}(s)$ is used for the auxiliary current instead of $W(s)$ because measuring $W(s)$ directly is difficult. Then the auxiliary current is given by

$$U_w(s) = \frac{K(s)}{t_o(s)} \hat{W}(s) \tag{19}$$

From (10), (17) and (19),

$$U(s) = \frac{K(s)\, w_0}{t_c(s)\{\, s + \sigma - \boldsymbol{j}(\omega_z + \nu)\}}. \tag{20}$$

Additionally from (8) and (20),

$$X(s) = \frac{(s - \boldsymbol{j}\omega_z) W(s)}{t_c(s)\{\, s + \sigma - \boldsymbol{j}(\omega_z + \nu)\}} + \frac{(\sigma - \boldsymbol{j}\nu) W(s)}{t_o(s)\{\, s + \sigma - \boldsymbol{j}(\omega_z + \nu)\}}. \tag{21}$$

Using (20) to compute $[U]$ yields

$$[U] = 0 \tag{22}$$

Hence the control current synchronized with rotation converges to zero. However, the second term of the right hand in (21) shows that the relative angle falls unstable because of the unstable poles of the $t_o(s)$.

In order to recover stability, $t_o(s)$ is replaced to $t_o(\boldsymbol{j}\omega_z)$ in (19) as

$$U_w(s) = \frac{K(s)}{t_o(\boldsymbol{j}\omega_z)}\hat{W}(s) \tag{23}$$

Then from (11) (17) and (23),

$$U(s) = \frac{K(s)W(s)}{t_c(s)t_o(\boldsymbol{j}\omega_z)\{s+\sigma-\boldsymbol{j}(\omega_z+\nu)\}} \times\left[(\sigma-\boldsymbol{j}\nu)t_o(s)-\{s+\sigma-\boldsymbol{j}(\omega_z+\nu)\}t_o(\boldsymbol{j}\omega_z)\right] \tag{24}$$

From (8), (11) and (24),

$$X(s) = \frac{W(s)}{t_c(s)} \times\left[1+\frac{b_\theta K(s)(\sigma-\boldsymbol{j}\nu)}{t_o(\boldsymbol{j}\omega_z)\{s+\sigma-\boldsymbol{j}(\omega_z+\nu)\}}\right] \tag{25}$$

Using (23) to compute $[U]$ also yields $[U]=0$. In addition, (25) shows that the suspension system is stably.

Effect of Current Regulation Control

The effect of the current regulation control was tested in terms of orbits of the relative angle and the control current. The orbits of the relative angle and control current are shown in Figure 6 (a) and (b), respectively. The whirling motion of the rotor is reduced and compensated form the ellipsoid to the circle due to the current regulation control in (a). Additionally, The amplitude of control current is substantially reduced due to the current regulation control in (b). These results show that the current regulation control is realized.

Angular velocity measurement with the current regulation control when the turntable is not swung was carried out using the experimental setup as shown in Figure 2. The spectrums of the estimated angular velocity are shown in Figure 7. In both the spectrums about the *x*- and *y*-axes, the synchronized component with the rotation is reduced by approximately 70 % while the component due to exciting signal by the induction motor are almost same with and without the current regulation control. As a result, the beat component in the measurement bandwidth of the AMB-based gyroscopic sensor is reduced by approximately 80 %. Additionally, when the current regulation control is applied, other components that appear exceptionally as shown in Figure 4 (a) are also reduced about the *x*-axis.

The input-output characteristics of the AMB-based gyroscopic sensor were obtained experimentally using the setup as shown in Figure 2. The turntable is swung at the frequency of 0.1 Hz; the sampling time for the date store is 10^{-3} sec in these experiments. Figure 7 shows the input-output characteristics of the

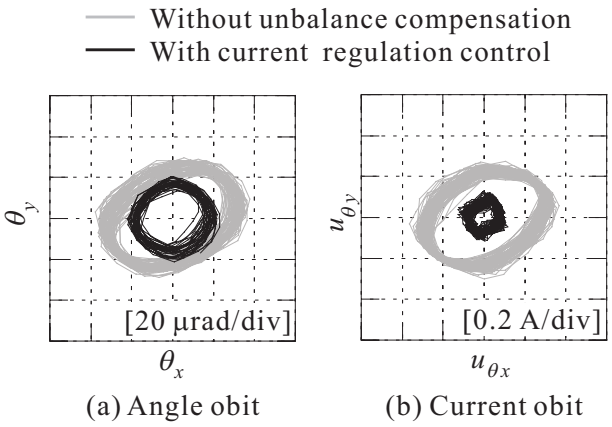

(a) Angle obit (b) Current obit

FIGURE 5: Effects of current regulation control in the angle and current orbit.

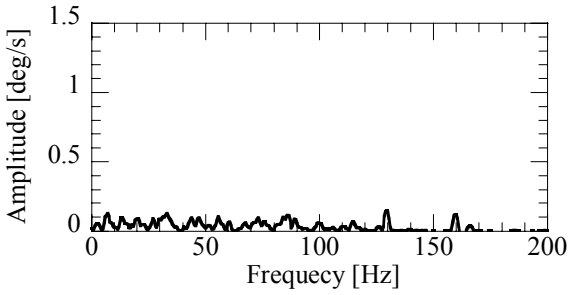

(a) *x*-axis

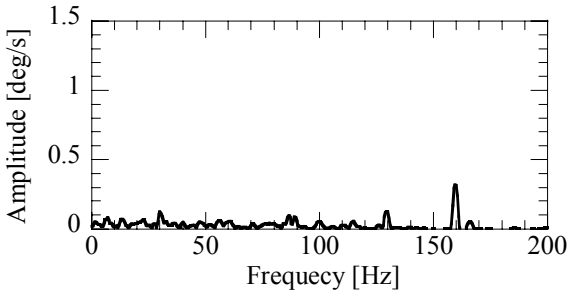

(b) *y*-axis

FIGURE 6: Spectrums of the estimated angular velocities with current regulation when the turntable is not swung.

AMB-based gyroscopic sensor. The noise levels of the sensor decease due to the current regulation control. In the range of the measurements, errors from the theoretical line with the current regulation control about the *x*- and *y*-axes are 0.15 % FS and 0.14 % FS, respectively while the errors without the current regulation control are 0.28 % FS and 0.27 % FS, respectively. Note that the full scale (FS) is ± 830 deg/s, the dynamic range of the AMB-based gyroscopic sensor. These results show that the current regulation control is effective in the case with input angular velocity to the

stator. Hence the current regulation control is suitable for the AMB-based gyroscopic sensor.

CONCLUSION

It was experimentally demonstrated that the estimated angular velocity by an AMB-based gyroscopic sensor contained several undesirable components due to rotor unbalance. Current regulation control was applied to the AMB-based gyroscopic sensor in order to eliminate the components. All of these components were reduced. In particular, the beat component in the measurement bandwidth is reduced by 80 %. In addition, it was shown that the current regulation control was efficacy in the case with input angular velocity to the stator and suitable for the AMB-based gyroscopic sensor.

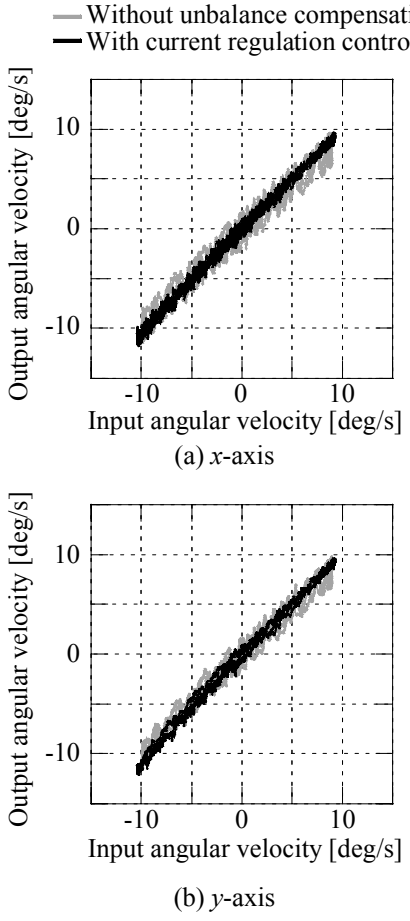

FIGURE 7: Input-output characteristics of the AMB-based gyroscopic sensor.

REFERENCE

1. Park, S. and Horowitz, R., "New Adaptive Mode of Operation for MEMS gyroscopes," *Trans. ASME, Journal of Dynamic Systems, Measurement and Control*, Vol.126, No.4, pp.800-810, 2004.

2. Piyabongkarn, D., Rajamani, R. and Greminger, M., "The Development of a MEMS Gyroscope for Absolute Angle Measurement," *IEEE Trans. Control Systems Technology*, Vol.13 No.2 pp.185-195, 2005.

3. A. Lawrence, Modern inertial technology: navigation, guidance, and control. New York: Springer-Verlag, 1992, pp.84-92.

4. R. H. Frazier, P. J. Gilinson, Jr and G. A. Oberbeck, *Magnetic and electric suspensions*. USA: The MIT press, 1974, pp.311-318.

5. Y. Maruyama, et al., "Basic Study on Gyroscopic Sensor using Active Magnetic Bearing," in *proc. The tenth International Symposium on Magnetic Bearings,* Martigny, Switzerland, 2006, New Fields in Magnetic Bearings and Industrial Applications, pp.57-60.

6. Y. Maruyama, et al. "An Application of Active Magnetic Bearing to Gyroscopic and Inertial Sensors," *Journal of System Design and Dynamics*, Vol. 2 No. 1, pp.155-164, 2008.

7. B. Shafai, S. Beale, P. LaRocca and E.Cusson, "Magnetic Bearing Control Systems and Adaptive Forced Blancing," *IEEE Control Systems*, Vol. 14, No.2, pp.4-13, 1994.

8. R. Herzog, P. Bühler, C. Gähler, R. Larsonneur, "Unbalance Compensation Using Generalized Notch Filters in the Multivariable Feedback of Magnetic Bearings," *IEEE Transactions on Control Systems Technology,* Vol.4, No.5, pp.580-586, 1996.

9. K. Y. Lum, V. T. Coppola, D. S. Bernstein, "Adaptive Autocentering Control for an Active Magnetic Bearing Supporting a Rotor with Unknown Mass Imbalance," *IEEE Transactions on Control Systems Technology,* Vol.4, No.5, pp.580-586, 1996.

10. T. Mizuno, T. Higuchi, "Design of Magnetic Bearing Controllers Based on Disturbance Estimation," in *Proc. 2nd International Symposium on Design and Synthesis*, Tokyo, Japan, 1990, pp.281-288.

11. Y. Maruyama, et al. "Estimation Method and Measurement Bandwidth of Gyroscopic Sensor using Active Magnetic Bearing," in *proc. Annual Conference of the IEEE Industrial Electronics Society*, Taipei, Taiwan, 2007, pp.2230-2235.